Journal of
Composites Science

MDPI

Article

Effect of Compatibilizer and Organoclay Reinforcement on Morphology and Properties of Styrene Copolymer Blends

Marianna Triantou, Marios Gavriel and Petroula A. Tarantili *

Laboratory of Polymer Technology, School of Chemical Engineering, National Technical University of Athens, 15780 Athens, Greece
* Correspondence: taran@chemeng.ntua.gr; Tel.: +30-2107723289

Abstract: The blending of polymers leads to materials with the desired combined properties. These properties can further be improved by the incorporation of compatibilizer, organoclay, or both. In the present manuscript, the effects of compatibilizer and organoclay, as well as their combined use on the rheological, thermal, and mechanical properties of styrene copolymer blends, is examined. Styrene-containing copolymers blends were prepared by melt-mixing in a twin screw extruder. The addition of SAN into ABS decreases its thermal stability, whereas it increases its tensile strength and modulus. The incorporation of organoclay in ABS/SAN blends increases their viscosity and slightly improves their thermal stability and significantly improves the tensile and storage moduli. In PC/SAN blends, the SAN copolymer increases the flow rate, as well as the tensile strength and modulus of PC, whereas it decreases the thermal stability. The addition of ABS-g-MAH compatibilizer in PC/SAN blends increases the melt viscosity and maximum decomposition rate temperature of SAN phase, while it leads to the earlier decomposition of the PC phase. The incorporation of organoclay reinforcement enhances the thermal decomposition resistance of thes SAN phase. The opposite effect was recorded for the PC phase. The addition of organoclay enhances the elastic modulus of PC/SAN hybrids.

Keywords: poly(styrene-co-acrylonitrile) copolymer; poly(acrylonitrile-butadiene-styrene) terpolymer; polycarbonate; organoclay; compatibilizer

Citation: Triantou, M.; Gavriel, M.; Tarantili, P.A. Effect of Compatibilizer and Organoclay Reinforcement on Morphology and Properties of Styrene Copolymer Blends. *J. Compos. Sci.* **2023**, *7*, 36. https://doi.org/10.3390/jcs7010036

Academic Editors: Francesco Tornabene and Vijay Kumar Thakur

Received: 9 November 2022
Revised: 19 December 2022
Accepted: 6 January 2023
Published: 11 January 2023

1. Introduction

Acrylonitrile-butadiene-styrene (ABS) is a styrene terpolymer produced by the grafting copolymerization of styrene and acrylonitrile into polybutadiene (PB) latex, resulting in a mixture of PB, PB grafted with acrylonitrile and styrene and styrene–acrylonitrile copolymer [1]. ABS is composed of a two-phase rubber-toughened plastic with a continuous poly(styrene-*co*-acrylonitrile) (SAN) glassy phase containing droplets of a dispersed polybutadiene latex [2]. The process that follows for manufacturing ABS is either bulk or emulsion polymerization [2]. The latter is mainly used industrially because it yields a fine graft control and a small submicron particle size distribution, which is more efficient for the toughening the SAN matrix [2].

Polycarbonate (PC) is an amorphous engineering thermoplastic with long linear chains of polyesters of carbonic acid and phenol, such as bisphenol A [3]. Polycarbonate exhibits superior dimensional stability, good electrical properties, thermal stability, flame retardancy, transparency, colorability, high-glossiness, and outstanding impact strength [4–6]. On the other hand, it is notch sensitive and difficult to process [4].

The blending of the existing polymers can be implemented more rapidly and economically than developing new polymers. Adding ABS to SAN leads to improved toughness. Adding SAN to PC results in a blend that is easier to process, has high modulus, and is less expensive than PC alone [7]. The main problems with PC/SAN alloys are their tendency to coalesce during processing. This can result in coarse structures, inferior material properties, and poor toughness [1]. The optimum composition for the best miscibility between SAN

and PC is about a 0.25 mole fraction of acrylonitrile (AN) [7]. Watkins and Hobbs [8] observed the minimum interfacial tension between PC and SAN at 15% AN.

Hanafy et al. [9] observed that the morphology of PC/SAN 70/30 blend is strongly influenced by AN content under the same processing conditions. The SAN particles are elongated in the flow direction for AN wt% 11–55; however, perfect circular domains are observed at AN wt% 74. The finest phase morphology is obtained at AN wt% 25, due to the maximum interfacial thickness attained at this concentration of AN. Additionally, at this AN load, the difference between the glass relaxation processes of the PC-rich and SAN-rich phases is minimum. The viscosity ratio plays a minor role in controlling the blend morphology. The morphology of the PC/SAN 70/30 blend containing 25 wt% AN strongly changes under shear flow; shear suppresses concentration fluctuations and promotes the miscibility of unlike domains. The shear memory can greatly suppress the coarsening behavior of the blend [10]. The shear memory cannot be erased after shear cessation, but is preserved even at high temperatures for a long time. After shear cessation, a rapid phase segregation process and a coarsening process occur immediately, which is a characteristic for the blend in the late stage of phase separation [10].

Takahashi et al. [11] concluded that the compatibility of SAN with PC, in 70/30 *w/ w* PC/SAN blends, is enhanced in extremely high shear rate processing. In particular, they observed that the apparent volume fraction of the spherical minor constituent (SAN) decreases with the shear rate. This means that SAN must be dispersed in PC, similar to a compatible constituent. SEM observations revealed that a dimple fracture of microsize took place on the SAN sphere, dispersed in the PC matrix. At the bottom of the dimple, a small particle (~50 nm), which is composed of PC, is present. This suggests that PC is dispersed in SAN, similar to a compatible constituent to the blend.

McLaughlin [12] observed that most of the compression-molded microstructure is predictable, based on a volume fraction: roughly spherical dispersions of the minor component within a matrix of the major component; or labyrinth, co-continuous structures for the case of approximately equal volume fractions. The co-continuous sheet-like injection-molded microstructure is maintained as the SAN level is reduced further to 20 wt%.

Lin et al. [13] found that the morphology of a PC/SAN 7/3 blend under low shear rate flow is an ellipsoidal structure, and above a critical shear rate, string-like morphology can be observed.

According to Wildes et al. [14], the morphology of multiphase polymer blends developed during processing is a complex function of blend composition, interfacial tension, rheological properties, shear conditions, and perhaps other attributes of the constituent material. The competing processes of drop break-up and coalescence during the melt processing determine the final morphology of these mixtures [14]. The above authors found that the particle size of the dispersed SAN phase in the 70/30 *w/w* PC/SAN blend is reduced with the addition of SAN-amine compatibilizer. The AN content of the SAN affects its interaction with both the PC and SAN-amine compatibilizers. Although the non-compatibilized 70/30 *w/w* PC/SAN blend with 25% AN presents a lower particle size of dispersed phase, compared to that of the corresponding blend with 32% AN, the degree of particle size reduction by adding SAN-amine is less for a blend with 25% AN. This can be attributed to the immiscibility between the SAN phase and the compatibilizer, which contain 25 and 32% AN, respectively. It has been shown that various SAN materials are only miscible with each other when the difference in AN content is approximately 4.5% or less.

Compatibilization of blends by incorporating the appropriate block or graft copolymers reduces the interfacial tension and retards the coalescence processes via steric stabilization. This makes it easier to achieve a finer dispersion of the dispersed phase, increases the interfacial strength, and improves the stability of morphology in the melt state. Relatively small and uniformly dispersed particles are usually advantageous for the properties of polymer blends [15].

Very interestingly, the incorporation of nanostructured layered silicates into polymeric matrices has been shown to induce interesting changes in the morphology of the resulting blends [16]. Nanocomposites of polymers with layer silicates are systems with a small amount of mineral clay particles with a thickness in the nanometer range, dispersed randomly and homogeneously in a polymer matrix [17]. The challenge in preparing high performance polymer nanocomposites (PNC) is to efficiently delaminate the clay sheets and properly disperse the sheets in the polymer matrix [17]. In the case of nanocomposites with a polymer blend matrix, their properties are strongly influenced by the domain structure, size, and interfacial interaction [18]. During the addition of clay into the polymer blend system, the coalescence of the droplets can be suppressed if the clay platelets are located at the phase boundary of the two polymers [17]. Meanwhile, the interfacial interaction between the immiscible phases can be enhanced [17]. Graphite [19], graphene [20], nanoplatelets, and carbon nanotubes [21–23] were also studied as reinforcement and compatibilizers in PC/SAN blends.

In this work, various blend combinations of SAN with compatible ABS and partially compatible PC were prepared by melt extrusion and tested to evaluate their rheological behavior and thermomechanical performance. Upgrading the performance of the ABS/SAN and PC/SAN blends was attempted with conventional compatibilization using ABS-g-MAH, in comparison and in combination with organoclay reinforcement. Although the PC/SAN blends have already been studied, the role of organoclay, alone or in combination with a compatibilizer, on these blends has not been examined extensively yet.

2. Materials and Methods

2.1. Materials

The copolymer poly(styrene–acrylonitrile) and the terpolymer poly(acrylonitrile–butadiene–styrene) were supplied by BASF, under the trade names Luran 378P and Terluran® GP-35, respectively. The polycarbonate used in this work was Makrolon 2805 by Bayer. Additionally, poly(acrylonitrile–butadiene–styrene) grafted with maleic anhydride, ABS-g-MAH (GPM400AB) was purchased by Ningbo Nengzhiguang New Materials Technology Co. Ltd., China, to be tested as conventional compatibilizer. The grafting ratio was 0.5–1%, and the melting index was 1 g/10 min at 230 °C, with a 2.16 kg load. The ABS-g-MAH was added to the PC/SAN blends at 10 wt%. Commercial montmorillonite clay (Cloisite® 30B), supplied by Rockwood Clay Additives GmbH, was also incorporated as a reinforcing nanofiller for the preparation of nanocomposites at concentrations of 2 phr. The organic modifier was methyl, tallow, bis-2-hydroxyethyl quaternary ammonium (MT2EtOH), in which the tallow consists of 65% C18, 30% C16, and 5% C14. The concentration of the organic modifier is 90 meq/100 g clay.

2.2. Preparation of Nanocomposites

2.2.1. Extrusion Molding

ABS/SAN and PC/SAN blends with compositions: 100/0, 70/30, 50/50, 30/70, and 0/100 *w*/*w* were prepared by melt-mixing, in a co-rotating twin-screw extruder, with L/D = 25 and 16 mm diameter (Haake PTW 16). A circular die with an opening of 2 mm diameter was mounted to the extruder, whereas the rotational speed of screws was 200 r/min. The extruder was heated at five zones, along the cylinder and the die. The temperature profile followed for ABS/SAN blends was 200–200–205–205–210–210 °C, while for PC/SAN blends was 250–250–255–255–260–260 °C. Before processing, SAN, ABS, and Cloisite 30B were dried in a vacuum oven at 80 °C for 4 h. PC and ABS-g-MAH were dried at 90 °C overnight, to avoid hydrolytic degradation. After melt-mixing, the obtained material, in continuous strands, was granulated using a Brabender knife pelletizer.

2.2.2. Injection Molding

Before injection, all the ABS/SAN blends and their nanocomposites were dried in a vacuum oven at 80 °C for 4 h. The PC/SAN blends and their nanocomposites were dried

at 90 °C for 6 h. Injection molding was performed in an ARBURG 221K ALLROUNDER machine, equipped with a screw of 25 mm diameter and clapping unit force of 350 kN. The mold was a two-cavity system, capable of producing dump-bell specimens for subsequent measurement of the tensile properties (ASTM D-638, specimens type IV). For all the ABS/SAN blends and their nanocomposites, the temperature profile was: 220–220–220–220–225 °C, with 1000 and 1150 bar injection pressures and 500 bar back pressure. For PC/SAN blends and their nanocomposites, the temperature profile was 260–260–260–260–265 °C, with 1250 and 1400 bar injection pressures and 800 bar back pressure.

2.3. Characterization

2.3.1. Melt Flow Index (MFI)

The MFI measurements were carried out according to ASTM D 1238 specification (procedure A), in a Kayeness Co. model 4004 capillary rheometer, at 200 °C with a 5 kg load for ABS/SAN blends and 260 °C with a 2.16 kg load for PC/SAN blends.

2.3.2. X-ray Diffractometer (XRD)

The dispersibility of silicate layers in the ABS/SAN and PC/SAN blends was evaluated in a Siemens 5000 apparatus X-ray diffractometer (40 kV, 30 mA), using CuKα irradiation with a wavelength of λ = 0.154 nm. The diffractograms were scanned in a 2θ range from 2–10°, with a rate of 0.01° s^{-1}. Samples for X-ray analysis were obtained from compression-molded plaques to avoid any preferred orientation of the clay reinforcement.

2.3.3. Thermogravimetric Analysis (TGA)

TGA measurements were performed in a Mettler Toledo (TGA-DTA model) thermal gravimetric analyzer. The tests were run with samples of 8–10 mg from 25 to 800 °C, at a heating rate of 10 °C min^{-1}, under nitrogen atmosphere.

2.3.4. Dynamic Mechanical Analysis (DMA)

For ABS/SAN blends, DMA measurements were carried out in an Anton Paar (model MCR 301) dynamic mechanical analyzer at a frequency of 1 Hz, with a heating rate of 5 °C min^{-1}, in the temperature range −120 and 150 °C. Samples prepared by injection molding were studied by this technique. For PC/SAN blends, DMA measurements were not feasible, due to their increased brittleness.

2.3.5. Differential Scanning Calorimetry (DSC)

DSC measurements were run in a Mettler Toledo model DSC 1 differential scanning calorimeter with pure indium as the calibration standard. Totals of 8–10 mg of the samples were heated from 30 to 200 °C to erase previous thermal history and then were cooled to 30 °C and heated again to 200 °C at a rate of 10 °C min^{-1}. All runs were conducted under nitrogen to limit thermooxidative degradation.

2.3.6. Tensile Test

Mechanical property testing of the injection-molded tensile specimens was performed according to ASTM D 638 in an Instron tensometer (4466 model) equipped with a load cell of maximum capacity of 10 kN, operating at grip separation speed of 50 mm min^{-1}. For each sample, four specimens were tested for duplication with the following dimensions: distance between grips 64 mm, width of narrow section 6 mm, and thickness 2.2 mm.

3. Results and Discussion

3.1. Melt Flow Index (MFI)

According to the results presented in Table 1, it is obvious that ABS shows a slightly higher melt flow index than SAN. Therefore, as the SAN content in the ABS/SAN blends increases, it is reasonable for the melt viscosity to increase. The MFI values tend to deviate positively from the additive rule. The incorporation of Cloisite 30B into the ABS/SAN

blends further increases the melt viscosity, compared to that of the non-reinforced blends. This can be attributed to the confinement of chain mobility, caused by the organoclay platelets and tactoids, in combination with the interactions among the polar groups of ABS and/or SAN and the oxygen groups of Cloisite 30B.

Table 1. Melt Flow Index of ABS/SAN and PC/SAN blends and their nanocomposites.

[2] Compat. (%)	OMMT (phr)	$MFI_{ABS/SAN}$ at 200 °C, 5 kg (g*10 min^{-1})				
		100/0	**70/30**	**50/50**	**30/70**	**0/100**
0	0	2.01 ± 0.16	2.03 ± 0.05 1.90 [1]	1.99 ± 0.07 1.82 [1]	1.85 ± 0.06 1.74 [1]	1.63 ± 0.08
	2	1.57 ± 0.11	1.79 ± 0.04	1.76 ± 0.02	1.60 ± 0.02	1.55 ± 0.08
		$MFI_{PC/SAN}$ at 260 °C, 2.16 kg (g*10 min^{-1})				
		70/30		50/50		30/70
0	0	9.64 ± 0.63 8.80 [1]		14.60 ± 0.52 10.83 [1]		15.53 ± 0.58 12.85 [1]
	2	10.48 ± 0.65		16.52 ± 0.81		14.91 ± 0.52
10	0	7.26 ± 0.36		9.61 ± 0.49		11.72 ± 0.78
	2	8.86 ± 0.33		10.45 ± 0.30		10.29 ± 0.41
PC (260 °C, 2.16 kg)	5.45 ± 0.33	SAN (260 °C, 2.16 kg)		15.89 ± 0.81	[2] Compat. (270 °C, 5 kg)	5.45 ± 0.33

[1] values according to the additive rule. [2] ABS-g-MAH.

In addition, from Table 1, it can be observed that PC has a much lower melt flow index than SAN. When SAN is added to the PC matrix, the MFI of the obtained blends increases, since their melt viscosity decreases up to 50/50 PC/SAN blends. Above this composition, the melt viscosity of PC/SAN blends becomes constant, almost obtaining the value of pure SAN. Similar observations were reported by Huang and Hung [7]. An interpretation of the deviation of melt viscosity for PC/SAN blends from the linear rule is that SAN dissolves more in the PC-rich phase than PC in the SAN-rich phase [7]. The dissolution of SAN into PC can be considered plasticization in the PC phase. In contrast, the minor PC phase in low content PC blends simply disperses into the SAN phase and does not increase viscosity until the PC itself becomes more or less a continuous phase.

The addition of compatibilizer in PC/SAN blends leads to an increase of melt viscosity, either due to the lower MFI of ABS-g-MAH or to a possible chemical reaction between the anhydride group of ABS-g-MAH and the terminal OH group of the PC [18].

The incorporation of nanoparticles into 70/30 and 50/50 *w*/*w* PC/SAN blends, with or without compatibilizer, tends to increase their flow rate. However, when the concentration of the PC becomes lower than that of SAN, a decrease in the flow rate occurs, because SAN seems to interact more efficiently with the organoclay nanoparticles.

3.2. X-ray Diffraction (XRD)

From Figure 1, the characteristic peak (001) of Cloisite 30B can be observed at about $2\theta = 5.08°$, corresponding to an inter-layer spacing of 1.74 nm. The XRD patterns of the Cloisite 30B/ABS/SAN and Cloisite 30B/PC/SAN blends in Figures 1 and 2, respectively, show that the peak corresponding to the (001) plane reflection of clay shifts to lower angles. The increased d-spacing suggests that the polymer chains intercalated into the gallery of nanoclay and increased the distance between the nanoclay layers [24], due to the strong shear during melt blending [25]. According to the literature [17], most of the clay platelets are located in the SAN phase, as well as in the phase boundaries of PC/SAN blends. The intercalation of SAN chains, present in ABS or SAN phase of ABS/SAN and PC/SAN blends, inside the clay galleries is driven by the interactions between the nitrile groups of the SAN phase and the hydroxyl groups of the organic modifier of nanofiller [26–29]. There is also a slight possibility of hydrogen bonding between the nitrile groups of SAN

and the ammonium cation of the intercalating agent [26]. The intercalation of PC chains in PC/SAN blends is caused by the hydrogen bonding between carbonyl groups in PC and the hydroxyl groups of the organic modifier of Cloisite 30B [30].

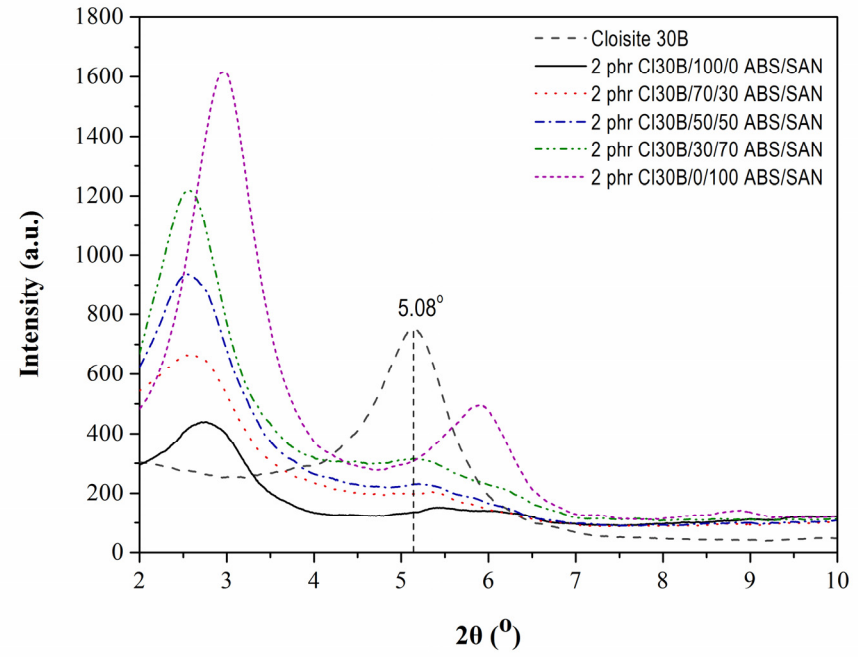

Figure 1. XRD patterns of Cloisite 30B and 2 phr Cloisite 30B/ABS/SAN blend nanocomposites.

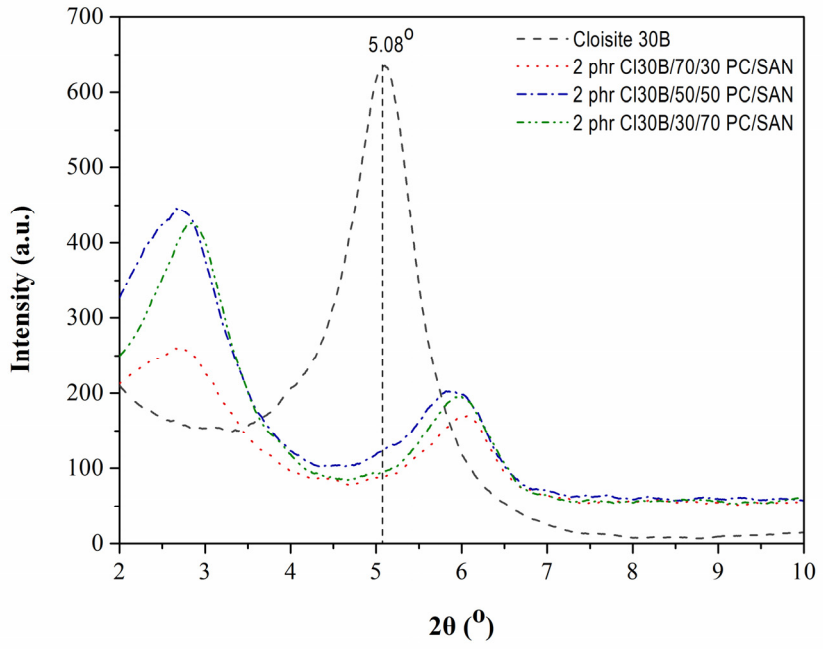

Figure 2. XRD patterns of Cloisite 30B and 2 phr Cloisite 30B/PC/SAN blend nanocomposites.

The secondary peak of nanocomposites shifts to higher angle values, compared to that of Cloisite 30B powder. It could arise from the partial disruption of parallel stacking of the clay platelets, possibly due to the decomposition of the organic modifier at high processing temperatures [24,31,32]. In addition to the above, the change of surrounding tension suppressed the clay layers and decreased the interlayer height of clay layers [33]. The secondary peak in Cloisite 30B/SAN nanocomposite is observed at a higher angle, compared to that of Cloisite 30B/ABS/SAN nanocomposites, probably due to the

higher torque values during the extrusion, which cause the greater decomposition of the organic modifier.

Therefore, mixed intercalated/delaminated nanocomposites were obtained for ABS/SAN and PC/SAN blends. Mixed intercalated/delaminated nanocomposites were obtained for ABS or SAN nanocomposites by other authors [34,35].

Comparing Figures 2 and 3, the effect of ABS-g-MAH compatibilizer on the degree of organoclay intercalation for PC/SAN blends can be assessed. The addition of a compatibilizer does not seem to have any noticeable effect on the intercalation of polymer chains between the clay platelets. As a result, the (001) peak position and its intensity are not affected by the presence of a compatibilizer.

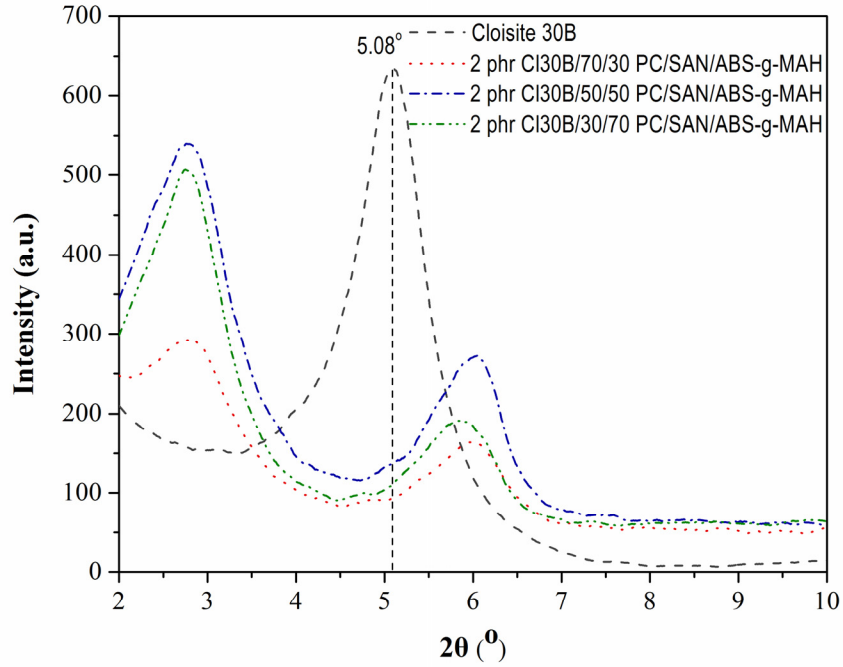

Figure 3. XRD patterns of Cloisite 30B and 2 phr Cloisite 30B/PC/SAN blend nanocomposites, compatibilized with 10% ABS-*g*-MAH.

3.3. Thermogravimetric Analysis (TGA)

The thermal stability of the ABS/SAN and PC/SAN blends was investigated using thermogravimetric analysis. ABS is more stable than SAN, as it presents higher onset decomposition temperature (T_{onset}) and maximum reaction rate temperature (T_{peak}). However, the former polymer leaves a lower decomposition residue at 800 °C. The thermal decomposition of ABS/SAN blends takes place in one stage. The increase of SAN content in ABS/SAN blends shifts their thermal decomposition to lower temperatures (Figure 4). The T_{onset} of blends nearly follow the additive rule, whereas the T_{peak} shows a negative deviation from this rule.

The incorporation of organoclay in ABS/SAN blends slightly improves their thermal stability, mainly at a composition of 30/70 *w*/*w*, as the concentration of the elastomeric nonpolar phase, which does not interact with the nanofiller, is lower. The increase in thermal stability of ABS/SAN nanocomposites can be attributed to the "labyrinth" effect of clay layers. Since the layers of organo-modified silicate are impermeable to the small molecules generated during the thermal decomposition process, the decomposition products have to take a long way around the clay layers [36–38]. The improvement of thermal stability is also ascribed to the protection of polymer chains intercalated into the clay galleries and to the confinement of their movements [38]. The "barrier" effect of clay [29,39] and the formation of char on the composite surface insulate the underlying material and inhibit the

escape of volatile products generated during thermal decomposition [29]. An increase in residue is recorded in ABS/SAN nanocomposites, compared to the non-reinforced blends (Figure 4).

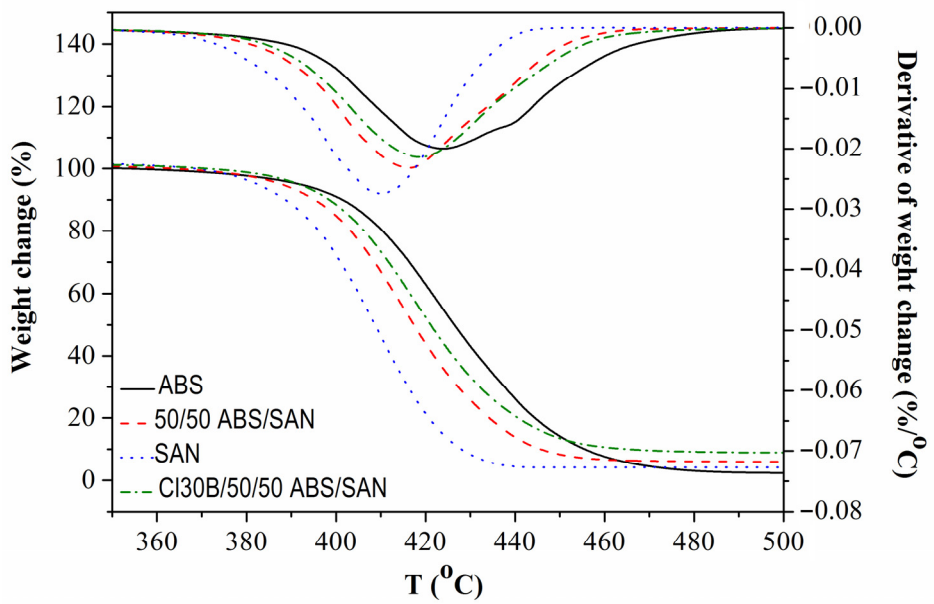

Figure 4. TGA and DTG curves for ABS, SAN, and 50/50 *w*/*w* ABS/SAN blend and its nanocomposite.

PC presents much higher thermal stability than SAN, as its thermal decomposition characteristics (T_{onset}, T_{peak}, and residue) are superior to those of SAN. The addition of 30% SAN in PC causes a reduction of T_{onset} at about 100 °C (Table 2). The further addition of SAN leads to a further decrease of T_{onset}, up to 50/50 *w*/*w* PC/SAN blends. The T_{onset} presents a significant negative deviation from the additive rule. The incorporation of ABS-g-MAH in PC/SAN blends does not have any noticeable effect in T_{onset}. The addition of Cloisite 30B has a positive effect on this value, mainly at 50/50 and 30/70 *w*/*w*, in which the SAN phase that interacts with the organoclay increases.

Table 2. Onset decomposition temperature (T_{onset}) of non-compatibilized and compatibilized (with ABS-g-MAH) PC/SAN blends and their nanocomposites.

[2] Compat. (%)	OMMT (phr)	T_{onset} (°C)			
		70/30	50/50	30/70	
0	0	405.3 ± 0.50 470.0 [1]	388.7 ± 0.05 447.4 [1]	393.7 ± 1.38 424.8 [1]	
	2	409.6 ± 1.21	403.3 ± 0.32	403.0 ± 0.25	
10	0	403.2 ± 1.05	394.3 ± 1.52	393.1 ± 0.40	
	2	406.4 ± 0.01	404.2 ± 1.22	402.5 ± 0.29	
PC	503.8 ± 0.79	SAN	391.0 ± 0.40	[2] Compat.	404.7 ± 1.60

[1] values according to the additive rule. [2] ABS-g-MAH.

The thermal decomposition of PC/SAN blends is a two-stage process, as suggested by the two peaks in Figure 5. The first peak corresponds to SAN phase, whereas the second corresponds to that of PC. The area of the two peaks depends on the proportion of the two components in the blend. The T_{peak} of the SAN phase in PC/SAN blends is higher than that of neat SAN and decreases as the SAN content increases. The T_{peak} of the PC phase in PC/SAN blends is lower than that of pure PC.

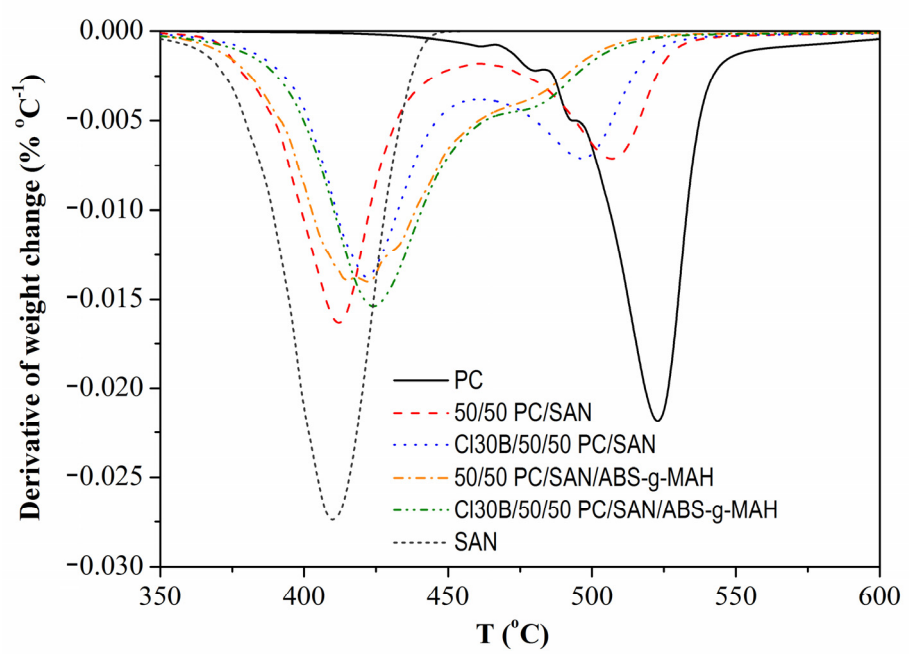

Figure 5. Derivative of weight change versus temperature for PC, SAN, and 50/50 *w*/*w* PC/SAN blends.

Adding an ABS-g-MAH compatibilizer in PC/SAN blends increases the T_{peak} of the SAN phase (Figure 5), mainly at 70/30 *w*/*w* blend composition. The thermal decomposition of the PC phase in 70/30 and 50/50 PC/SAN/ABS-g-MAH blends appears as a shoulder on the right side of the peak, whereas no peak or "shoulder" is observed in the 30/70 *w*/*w* blend.

Moreover, the incorporation of nanoparticles in the PC/SAN blends significantly increases the T_{peak} of the SAN phase and leads to the completion of thermal decomposition of this phase at higher temperatures. On the contrary, it decreases the T_{peak} of the PC phase, whose thermal decomposition is completed at lower temperatures. The combined use of ABS-g-MAH and organically modified montmorillonite in PC/SAN blends further increases the T_{peak} of the SAN phase.

The residue at 800 °C decreases as the SAN content in PC/SAN blends increases (Table 3). The addition of organoclay slightly decreases the residue, while a more significant decrease occurs with the addition of ABS-g-MAH compatibilizer into the examined blends. As expected, the incorporation of organoclay into compatibilized blends results in higher amounts of residue, in comparison with the respective unreinforced blends. Interestingly, those amounts are smaller than those obtained from non-compatibilized samples, which suggests a synergistic effect of the compatibilizers on the decomposition process of the blends.

Table 3. Residue of non-compatibilized and compatibilized (with ABS-g-MAH) PC/SAN blends and their nanocomposites.

[2] Compat. (%)	OMMT (phr)	Residue (%)		
		70/30	50/50	30/70
0	0	18.51 ± 1.98 20.57 [1]	12.14 ± 1.06 15.89 [1]	11.37 ± 0.14 11.21 [1]
	2	18.41 ± 0.73	11.88 ± 0.66	10.08 ± 2.12
10	0	14.56 ± 0.98	7.72 ± 0.87	5.00 ± 1.84
	2	14.8 ± 1.28	10.96 ± 0.71	7.20 ± 0.04
PC	27.59 ± 0.12	SAN	4.19 ± 0.63	[2] Compat. 2.59 ± 0.67

[1] values according to the additive rule. [2] ABS-g-MAH.

3.4. Dynamic Mechanical Analysis (DMA)

ABS molding compounds consist of a continuous phase (matrix) of copolymers of styrene (or alkylstyrene) and acrylonitrile, in which butadiene forms the dispersed phase. Therefore, the ABS/SAN blend presents two glass transition temperatures, T_g, one corresponding to the rubber (PB) phase and the other to the thermoplastic (SAN) phase. The thermal transitions of the ABS/SAN blends, as derived from DMA experiments from G versus temperature plot, are presented in Figure 6. From this figure, it is observed that the T_g of PB in ABS/SAN blends slightly decreases as the SAN content in ABS/SAN blend increases. The T_g of the SAN phase in pure ABS was found in 99 °C, whereas that of pure SAN appears at 108 °C. For the ABS/SAN blends, a shift to higher temperatures of the glass transition of SAN is recorded as the SAN content increases.

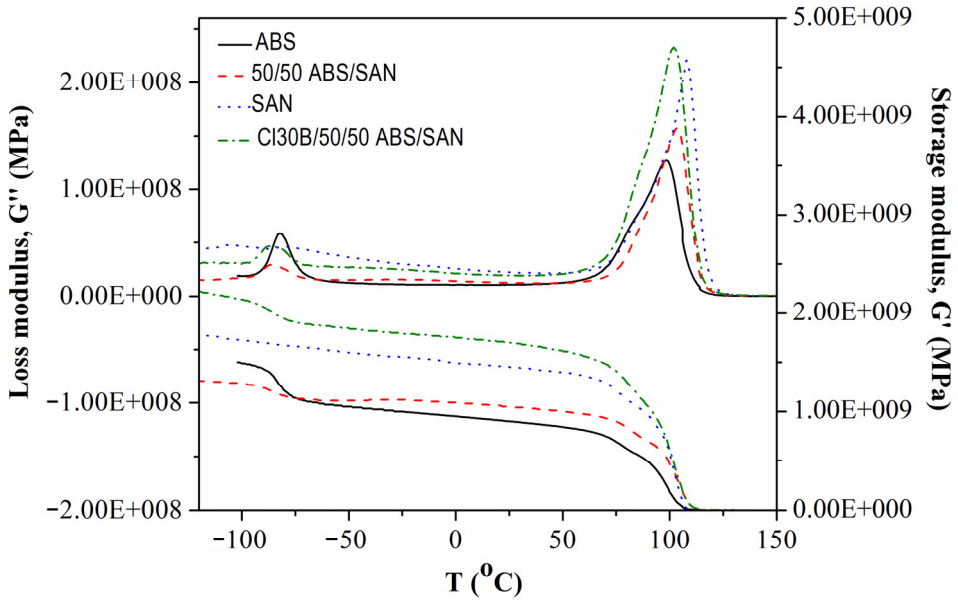

Figure 6. Storage modulus (G′) and loss modulus (G″) of ABS, SAN, 50/50 *w*/*w* ABS/SAN blend and its nanocomposite.

The addition of 2 phr organoclay does not have any noticeable effect on the T_g of PB and SAN phases of ABS/SAN blends. Similar observations have been recorded by other authors [40–43]. The filler acts as a reinforcing agent, limiting the chain mobility only at temperatures below T_g of SAN. In contrast to higher temperatures, the total softening of the SAN phase inhibits the action exerted by the clay [44]. The peaks' broadening can be attributed to the inhibition of the relaxation process within the composites. The presence of a high modulus nanofiller in the ABS/SAN system reduces the flexibility of the material by introducing constraints on the segmental mobility of the polymeric molecules at the relaxation temperatures. The loss modulus value in the transition region is much higher for the nanocomposites, compared to pure resin, due to the increase in internal friction that enhances energy dissipation [45].

Figure 6 presents the storage modulus, G′, of ABS/SAN blends versus temperature. It seems that SAN presents higher G′ than ABS in all the examined ranges of temperatures. The ABS/SAN blends show a lower storage modulus than that of pure ABS up to −80 °C. Above this temperature, the storage modulus of ABS/SAN blends is higher than that of pure ABS and lower than that of SAN. Additionally, it tends to increase by increasing the SAN content in the blend.

Incorporating organoclay nanoplatelets into ABS/SAN blends significantly improves their storage modulus (Figure 6). This behavior can be attributed to the toughness and the high aspect ratio L/D of clay nanoplatelets. Moreover, the interactions between the polymer matrix and the organic modification of nanoclay lead to sufficient clay dispersion,

which confines the polymeric chains motion between the clay galleries. The increase of the storage modulus by adding organoclay is more intense in systems with high SAN content. The greater AN content can induce greater intercalation [29] and stronger interactions with the nanofiller, due to its polarity. Mainil et al. [41] observed that the MMT/SAN nanocomposite presented a higher storage modulus of Cloisite 30B/SAN nanocomposite, although with a better dispersion of OMMT into the polymer matrix and their better interfacial adhesion. This is because the expected mechanical strengthening of the SAN matrix was partially counter-balanced by the soft Cloisite 30B organomodifier molecules located at the interphase.

3.5. Differential Scanning Calorimetry (DSC)

Due to the increased brittleness of PC/SAN injection-molded specimens, the observation of their thermal transitions was not feasible using dynamic mechanical analysis. Thus, the thermal transitions of this blend were recorded by differential scanning calorimetry. The glass transition temperatures, T_g, of pure SAN and PC were determined at 109.6 °C and 142.8 °C, respectively. Hanafy et al. [9] observed that the T_g of pure SAN is independent of the SAN composition.

As can be seen in Figure 7, the PC/SAN blend exhibits two glass transitions. The first corresponds to the SAN-rich phase and appears at temperatures slightly higher than that of pure SAN. The second corresponds to the PC-rich phase and appears at temperatures that are slightly lower, compared to that of pure PC. The fact that the glass transition temperatures of the two phases of the blend are closer to each other than those of pure components has been considered an indication of partial miscibility [46]. It can be seen from the literature [9,47,48] that the miscibility of the two polymers depends on the AN content of the SAN phase and the proportion of the two components in the blend. The optimum content of AN in the SAN phase ranges from 25% to 30%.

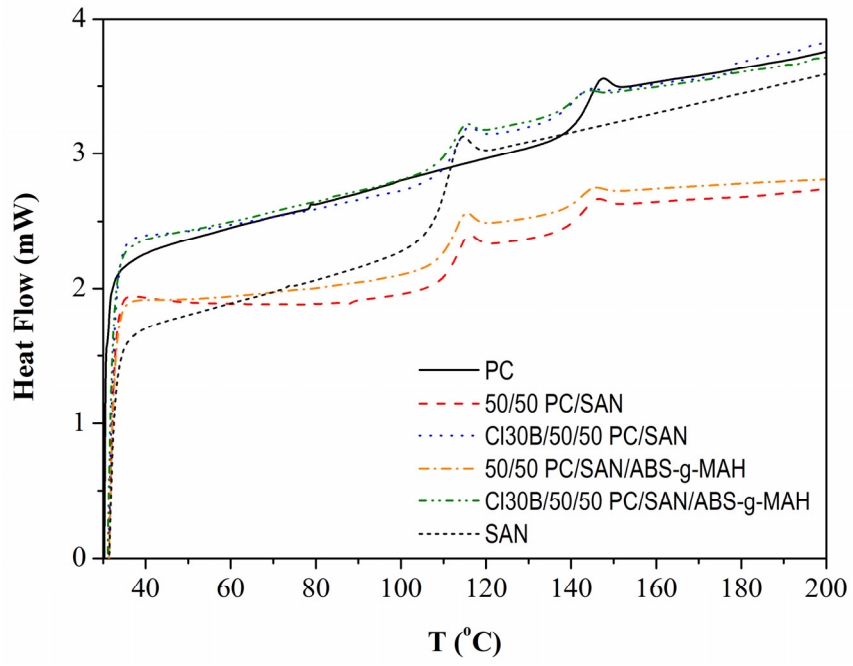

Figure 7. DSC heating curves of PC, SAN and 50/50 *w*/*w* PC/SAN blends.

The T_g of the SAN phase tends to increase as the SAN content in the blend decreases. The T_g of the PC phase slightly decreases with increasing SAN concentrations in the PC/SAN blends. Similar observations were recorded by Kim et al. [49]. Hanafy et al. [9] observed that the shift of the glass relaxation process of the SAN-rich phase to a higher temperature is much higher than that of the PC-rich phase to a lower temperature in the

PC/SAN 70/30 blend, indicating that PC is more soluble in SAN than SAN in PC. This behavior was also observed in our experiments for PC/SAN blends at 70/30 and 50/50 w/w, but not at the composition of 30/70 w/w. Hanafy et al. [10] found that the T_g of the SAN-rich phase in the PC/SAN 70/30 blend is almost constant for all the range of shear rates, indicating that no more PC is dissolved into the SAN-rich phase. In contrast, the T_g of the PC-rich phase is shifted to lower temperatures with increasing applied shear rate values. The reason for this shift is attributed to the fact that some amount of SAN is dissolved in the PC under shear forces.

The addition of ABS-g-MAH in the PC/SAN blend causes a slight decrease in both T_gs. Furthermore, the incorporation of nanoparticles in non-compatibilized and compatibilized PC/SAN blends tends to reduce the T_gs of both phases, mainly that of the PC phase.

For further investigation of the phase behavior of PC/SAN blends, a method attempting to directly assess the amount of PC dissolved in the SAN phase and vice versa was used. It assumes the Fox equation would describe the T_g composition relation, if PC were fully miscible with SAN. By inverting the Fox equation:

$$\frac{1}{T_g} = \frac{w_{SAN}}{T_{g,SAN}} + \frac{(1 - w_{SAN})}{T_{g,PC}} \quad (1)$$

the weight fraction of SAN in either the styrenic or polycarbonate phase can be calculated as:

$$w_{SAN} = \frac{T_{g,SAN}(T_{g,PC} - T_g)}{T_g(T_{g,PC} - T_{g,SAN})} \quad (2)$$

by inserting the T observed for the phase interest [50,51].

The T_g values for PC and SAN-rich phases can help us determine the weight fractions of each phase, according to Equations (1) and (2), above. The calculated volume fractions are presented in Table 4. The weight fraction of SAN in the PC phase and PC in the SAN phase decrease, increasing the contents of PC and SAN, respectively, in the blend. Additionally, the weight fraction of SAN in the PC phase tends to be increased by the addition of compatibilizer, whereas the weight fraction of PC in the SAN phase decreases. The incorporation of nanofiller increases the weight fraction of SAN in the PC phase, whereas it decreases the weight fraction of PC in the SAN phase. This behavior might be attributed to stronger interactions between SAN and OMMT, in comparison with those taking place in the system PC and OMMT. It seemed that, in the 30/70 w/w PC/SAN blend, SAN is more soluble in PC than PC is in SAN, whereas the opposite effect occurred with 50/50 and 70/30 w/w blends. Keitz et al. [48] found that polycarbonate is more soluble in SAN than SAN is in polycarbonate.

Table 4. Weight fraction of SAN in PC phase (w_{SAN}) and PC in SAN phase w_{PC}, based on T_g values from DSC.

Compat. (ABS-g-MAH) (%)	OMMT (phr)	w_{SAN} in PC Phase			w_{PC} in SAN Phase		
		PC/SAN (w/w)					
		70/30	50/50	30/70	70/30	50/50	30/70
0	0	0.03	0.03	0.07	0.10	0.09	0.03
	2	0.11	0.10	0.16	0.03	0.07	0.02
10	0	0.05	0.05	0.08	0.04	0.04	0.01
	2	0.12	0.09	0.16	0.04	0.02	0.01

3.6. Tensile Properties

According to Table 5, the SAN displays two times higher tensile strength, in comparison with ABS. Furthermore, it presents a higher Young's modulus and lower tensile strain than ABS.

Table 5. Tensile properties of ABS/SAN blends and their nanocomposites.

OMMT (phr)	ABS/SAN (*w*/*w*)				
	100/0	**70/30**	**50/50**	**30/70**	**0/100**
	Tensile strength (MPa)				
0	46.77 ± 0.22	59.85 ± 0.25 59.61 [1]	66.58 ± 1.10 68.18 [1]	75.21 ± 0.30 76.74 [1]	89.58 ± 1.78
2	47.19 ± 0.43	62.08 ± 2.30	67.24 ± 0.00	74.87 ± 0.33	[2]
	Young's modulus (MPa)				
0	2105.42 ± 70.44	2321.47 ± 137.25 2284.77 [1]	2579.22 ± 16.43 2404.34 [1]	2822.32 ± 106.97 2523.90 [1]	2703.25 ± 108.87
2	2321.47 ± 137.25	2746.40 ± 138.33	3111.11 ± 94.30	3197.77 ± 52.50	[2]
	Tensile strain (%)				
0	13.21 ± 3.15	10.68 ± 1.63 10.57 [1]	8.90 ± 0.55 8.81 [1]	8.01 ± 0.91 7.05 [1]	4.41 ± 0.28
2	5.67 ± 1.46	5.29 ± 0.23	8.48 ± 1.24	6.49 ± 0.37	[2]

[1] values according to the additive rule. [2] injection molding was not feasible, due to the increased fragility of samples.

The tensile strength and Young's modulus are improved as the SAN content in the blend increases, whereas the tensile strain decreases. The tensile strength and the strain at breaking point of ABS/SAN blends nearly follow the rule of mixtures, whereas the elastic modulus shows a positive deviation. Yamakawa et al. [2] observed that the yield stress decreases with increasing rubber content, as the rubber particles under hydrostatic stress may cavitate and trigger the matrix-toughening mechanism, thereby allowing the material to yield at lower tensile stress levels. Additionally, the above researchers observed that the stiffness of the blends increases by increasing the SAN content, as the SAN phase is much stiffer than that of the rubber phase [2].

The addition of OMMT in pure SAN did not permit its injection molding, due to the increased brittleness of samples. Bourbigot et al. [34] observed that the Young's modulus of SAN nanocomposites increases linearly as a function of the MMT concentration, but concurrently, the tensile strength and strain at break decrease. The incorporation of organoclay does not obviously affect the tensile strength, whereas it increases the Young's modulus significantly. The higher modulus of nanocomposites might be due to the higher modulus of the filler and to limitations in the deformability of polymeric chains penetrating the silicate galleries. Furthermore, a decrease in tensile strain was recorded, mainly in ABS and 70/30 ABS/SAN nanocomposites, maybe due to the increase of the elastomeric phase, which has no affinity with the organoclay.

From Table 6, it is observed that SAN presents better tensile properties than PC, in terms of tensile strength and Young's modulus. It is also characterized by lower tensile strain at break. The tensile strength and Young's modulus of PC/SAN blends increase by increasing SAN content and present a positive deviation from the additive rule. In fact, the 30/70 *w*/*w* PC/SAN blend exhibits higher Young's modulus than pure SAN. Similar results were reported by Huang and Hung [7].

Table 6. Tensile properties of non-compatibilized and compatibilized (with ABS-g-MAH) PC/SAN blends and their nanocomposites.

Compat. (%)	OMMT (phr)	PC/SAN (*w*/*w*)		
		70/30	**50/50**	**30/70**
		Tensile strength (MPa)		
0	0	76.07 ± 0.51 72.18 [1]	81.13 ± 0.78 77.15 [1]	83.62 ± 4.29 82.12 [1]
	2	76.73 ± 0.68	74.77 ± 6.56	[2]
10	0	66.31 ± 0.48	71.17 ± 0.32	75.34 ± 0.90
	2	68.98 ± 0.47	74.04 ± 0.43	73.03 ± 0.13
PC	64.72 ± 0.52		SAN	89.58 ± 1.78
		Young's modulus (MPa)		
0	0	2417.84 ± 58.03 2164.30 [1]	2699.19 ± 138.71 2318.29 [1]	3087.00 ± 120.98 2472.27
	2	2850.57 ± 160.45	3298.55 ± 86.69	[2]
10	0	2391.91 ± 66.24	2654.94 ± 9.52	2589.24 ± 83.41
	2	2570.75 ± 97.07	2593.40 ± 53.90	2837.91 ± 46.33
PC	1933.32 ± 87.28		SAN	2703.25 ± 108.87
		Tensile strain (%)		
0	0	27.74 ± 1.86 17.12 [1]	4.99 ± 0.32 13.49 [1]	3.76 ± 1.03 9.86 [1]
	2	32.1 ± 4.74	4.01 ± 0.88	[2]
10	0	33.28 ± 3.28	13.34 ± 2.20	10.58 ± 0.2
	2	37.24 ± 3.79	10.98 ± 1.02	3.25 ± 0.98
PC	22.57 ± 3.04		SAN	4.41 ± 0.28

[1] values according the additive rule. [2] injection molding was not feasible, due to the increased fragility of samples.

According to Skochdopole et al. [47], the AN content of the SAN phase affects the proportion in which the tensile strength and the elongation at break show a peak.

The addition of ABS-g-MAH decreases the tensile strength and the Young's modulus, mainly at the system 30/70 PC/SAN *w*/*w*, but increases the tensile strain, probably due to the increase of elastomer phase. Yin et al. [1] observed a decrease in tensile strength and an increase in tensile strain, with an increase of styrene-ethylene-butadiene-styrene block copolymer (SEBS) content. Additionally, they found that the addition of SEBS, SEEPS (styrene-ethylene-ethylene-propylene-styrene block copolymer), or ABS in the PC/SAN blends has a similar influence on the tensile strength. SEBS and SEEPS have similar elongation at break, while ABS has the lowest. This can be attributed to the deterioration of compatibility between SAN and PC phases, which is caused by the addition of ABS. ABS exists mainly in the SAN phase, whereas SEBS is distributed not only in the SAN phase, but also in the PC, leading to a co-continuous structure.

The incorporation of Cloisite 30B increases the Young's modulus of non-compatibilized and compatibilized blends. This is due to the intercalation of polymer chains into the galleries of organoclay and their possible interactions. Lin et al. [17] attributed the increase of Young's modulus caused by increasing clay loading to the increase of the exfoliated component in the SAN phase, as formed by the high shear forces during extrusion. The increase in exfoliation enhances the possible interactions between the clay platelets and polymer matrix.

4. Conclusions

From the above study, and specifically from the discussion of results, some interesting conclusions can be drawn.

First, the changes in the melt flow characteristics of the blends can be due to the additivity of the different viscosities of their components, as well as to a plasticization effect caused by the low viscosity polymers. Additionally, the interactions with the fillers also seem to have an influence. X-ray diffraction analysis was found to be a useful tool for the characterization of the microstructure of reinforced blends and showed that mixed intercalated/delaminated nanocomposites were obtained for ABS/SAN and PC/SAN blends. In addition, some interesting results obtained from TGA analysis suggest that a synergistic effect of the compatibilizers on the decomposition process of the blends takes place, whereas DMA revealed that the addition of 2 phr organoclay does not have any significant effect on the T_g of PB and SAN phases of ABS/SAN blends, but clearly improves the storage modulus of ABS/SAN blends. It also should be noted that the determination of the T_g values via DSC tests allows for the calculation of the weight fraction of the different phases in the polymeric blend, which is of importance for their performance. Finally, the mechanical tests showed that the tensile strength and Young's modulus are improved with SAN concentration, whereas the tensile strain decreases. The tensile strength and the ultimate strain of ABS/SAN blends nearly follow the rule of mixtures, whereas the elastic modulus presents some higher values than those deriving from the rule. The addition of ABS-g-MAH decreases the tensile strength and modulus, mainly of the system 30/70 PC/SAN w/w, but increases the tensile strain, probably due to the increase of elastomer phase.

The blending of polymers permits us to combine the properties of their components. In the ABS/SAN blends, the SAN copolymer enhances the mechanical properties of ABS, while the latter contributes to the higher thermal stability of the former. Regarding the PC/SAN blends, the SAN copolymer improves the flow rate of PC, while PC offers higher thermal stability. The thermal decomposition of the respective blends takes place in two stages. The increase in the glass transition temperature of the SAN phase is more intense than the decrease of the glass transition temperature of the PC phase in 70/30 and 50/50 w/w PC/SAN systems. This is due to the higher dissolution of PC molecules in part of the SAN copolymer. The opposite is observed in the 30/70 w/w PC/SAN blend.

PC/SAN blends are partially miscible, and the addition of a suitable compatibilizer may enhance their performance. The addition of ABS-g-MAH does not seem to have any positive effect on the compatibilization of PC/SAN blends and, consequently, on their properties. In particular, it increases their melt viscosity and leads to the earlier decomposition of the PC phase in the examined blends. Moreover, it decreases the tensile strength and Young's modulus, mainly at the composition 30/70 PC/SAN w/w. However, it increases the T_{peak} of the SAN copolymer phase and the tensile strain.

The incorporation of organoclay in ABS/SAN and PC/SAN blends seems to enhance their thermal and mechanical properties, due to its interactions mainly with the SAN phase, which leads to intercalated/exfoliated nanocomposites. In the ABS/SAN blends, the organoclay increases their melt viscosity, improves their thermal stability, and increases the storage and elastic modulus.

In PC/SAN blends, the incorporation of organoclay reinforcement enhances the thermal decomposition resistance of the SAN phase, whereas the opposite effect was recorded for the PC phase. Furthermore, it increases the Young's modulus of non-compatibilized and compatibilized PC/SAN hybrids. Except the reinforcement offered to these blends, it acts as a compatibilization agent as it increases the weight fraction of the SAN in the PC phase.

In conclusion, the higher chemical affinity of the reinforcing filler with the SAN phase in the ABS/SAN and PC/SAN blends affects their performance. An appropriate modification of the reinforcing filler, capable of increasing its interaction with the PC phase, as well, would improve the miscibility of the blend components and, thus, the blend properties.

Author Contributions: Conceptualization, M.T. and P.A.T.; methodology, M.T.; validation, M.T. and P.A.T.; investigation, M.T. and M.G.; resources, P.A.T.; writing—original draft preparation, M.T.; writing—review and editing, M.T. and P.A.T.; supervision, P.A.T. All authors have read and agreed to the published version of the manuscript.

Funding: This research received no external funding.

Data Availability Statement: Not applicable.

Acknowledgments: We would like to acknowledge the Bodossaki Foundation for the scholarship to Triantou PhD. Special thanks go to Dimitrios Korres for assistance with the DSC and TGA experiments.

Conflicts of Interest: The authors declare no conflict of interest.

References

1. Yin, N.; Zhang, Y.; Zhang, Y.; Zhang, X.; Zhou, W. Preparation and properties of PC/SAN alloy modified with styrene-ethylene-butylene-styrene block copolymer. *J. Appl. Polym. Sci.* **2007**, *106*, 637–643. [CrossRef]
2. Yamakawa, R.S.; Correa, C.A.; Hage Jr., E. Influence of acrylonitrile-butadiene-styrene (ABS) morphology and poly(styrene-co-acrylonitrile) (SAN) content on fracture behavior of ABS/SAN blends. *J. Appl. Polym. Sci.* **2004**, *92*, 2606–2611. [CrossRef]
3. Cândido, L.; Kindlein, W.; Demori, R.; Carli, L.; Mauler, R.; Oliveira, R. The recycling cycle of materials as a design project tool. *J. Clean. Prod.* **2011**, *19*, 1438–1445. [CrossRef]
4. Nigam, I.; Nigam, D.; Marthur, G.N. Effect of Rubber Content of ABS on Properties of PC/ABS Blends. I. Rheological, Mechanical, and Thermal Properties. *Polym. Plast. Technol. Eng.* **2005**, *44*, 815–832. [CrossRef]
5. Statler, D.; Stajduhar, E.; Gupta, R. Flame retardancy of polycarbonate upon repeated recycling. *J. Fire Sci.* **2008**, *26*, 331–350. [CrossRef]
6. Sokol, R.; Nedbal, J.; Fähnrich, J.; Ilavský, M.; Kolařík, J. Effect of interphase interactions on the dielectric behaviour of polycarbonate/poly(styrene-co-acrylonitrile) blends. *Polym. Bull.* **2000**, *44*, 555–562. [CrossRef]
7. Huang, J.C.; Hung, C.P. Melt Viscosities and Mechanical Properties of PC/SAN Blends. *Int. J. Polym. Mater.* **2000**, *46*, 683–694. [CrossRef]
8. Watkins, V.H.; Hobbs, S.Y. Determination of interfacial tensions between BPA polycarbonate and styrene-acrylonitrile copolymers from capillary thread instability measurements. *Polymer* **1993**, *34*, 3955–3959. [CrossRef]
9. Hanafy, G.M.; Madbouly, S.A.; Ougizawa, T.; Inoue, T. Effects of AN-contents and shear flow on the miscibility of PC/SAN blends. *Polymer* **2004**, *45*, 6879–6887. [CrossRef]
10. Hanafy, G.M.; Madbouly, S.A.; Ougizawa, T.; Inoue, T. Effect of shear history on the morphology and coarsening behaviour of polycarbonate/poly(styrene-co-acrylonitrile) blend. *Polymer* **2005**, *46*, 705–712. [CrossRef]
11. Takahashi, H.; Matsuoka, T.; Ohta, T.; Fukumori, K.; Kurauchi, T.; Kamigaito, O. Enhanced Compatibility of SAN and PC in Their Blends Exposed to Extremely High Shear Field. *J. Appl. Polym. Sci.* **1988**, *36*, 821–1831. [CrossRef]
12. McLaughlin, K.W. The Influence of Microstructure on the Dynamic Mechanical Behavior of Polycarbonate/Poly(Styrene-Co-Acrylonitrile) Blends. *Polym. Eng. Sci.* **1989**, *29*, 1560–1568. [CrossRef]
13. Lin, D.; Cheng, H.; Zou, F.; Ning, W.; Han, C.C. Morphology evolution of a bisphenol A polycarbonate/poly(styrene-co-acrylonitrile) blend under shear and after shear cessation. *Polymer* **2012**, *53*, 1298–1305. [CrossRef]
14. Wildes, G.; Keskkula, H.; Paul, D.R. Morphology of PC/SAN Blends: Effect of Reactive Compatibilization, SAN Concentration, Processing, and Viscosity Ratio. *J. Polym. Sci. Part B Polym. Phys.* **1999**, *37*, 71–82. [CrossRef]
15. Wildes, G.; Keskkula, H.; Paul, D.R. Fracture characterization of PC/ABS blends: Effect of reactive compatibilization, ABS type and rubber concentration. *Polymer* **1999**, *40*, 5609–5621. [CrossRef]
16. Utracki, L.A. *Clay-Containing Polymeric Nanocomposites*; Rapra Technology Limited: Crewe, UK, 2004; Volume 1.
17. Lin, D.; Boschetti-de-Fierrro, A.; Alexandre, M.; Abetz, C.; Böttcher, H.; Abetz, V.; Urbanczyk, L.; Jérôme, C.; Han, C.C. Morphology and mechanical properties of bisphenol A polycarbonate/poly(styrene-co-acrylonitrile) blends based clay nanocomposites. *Compos. Sci. Technol.* **2011**, *71*, 1893–18971. [CrossRef]
18. Balakrishnan, S.; Neelakantan, N.R.; Saheb, D.N.; Jog, J.P. Rheological and morphological behavior of blends of polycarbonate with unmodified and maleic anhydride grafted ABS. *Polymer* **1998**, *39*, 5765–5771. [CrossRef]
19. Paiva, M.C.; Cunha, E.P.; Voigt, O.; Liebscher, M.; Simon, F.; Pionteck, J.; Pötschke, P. Melt mixing functionalized graphite nanoplates into PC/SAN blends. *AIP Conf. Proc.* **2017**, *1914*, 030019.
20. Liebscher, M.; Blais, M.-O.; Pötschke, P.; Heinrich, G. A morphological study on the dispersion and selective localization behavior of graphene nanoplatelets in immiscible polymer blends of PC and SAN. *Polymer* **2013**, *54*, 5875–5882. [CrossRef]
21. Liebscher, M.; Tzounis, L.; Pötschke, P.; Heinrich, G. Influence of the viscosity ratio in PC/SAN blends filled with MWCNTs on the morphological, electrical, and melt rheological properties. *Polymer* **2013**, *54*, 6801–6808. [CrossRef]
22. Liebscher, M.; Domurath, J.; Krause, B.; Saphiannikova, M.; Heinrich, G.; Pötschke, P. Electrical and melt rheological characterization of PC and co-continuous PC/SAN blends filled with CNTs: Relationship between melt-mixing parameters, filler dispersion, and filler aspect ratio. *J. Polym. Sci. Part B Polym. Phys.* **2018**, *56*, 79–88. [CrossRef]

23. Lee, J.W.; Lee, S.; Kim, H. Effect of mixing protocol on the morphology development of multi-walled carbon nanotubes incorporated ternary blends of polycarbonate, styrene-acrylonitrile, and poly(methyl methacrylate) in a twin screw extruder. *Korea Aust. Rheol. J.* **2021**, *33*, 143–150. [CrossRef]
24. Feyz, E.; Jahani, Y.; Esfandeh, M.; Ghafelehbashi, M.; Jafari, S.H. Study of the Viscoelastic Properties of PC/ABS Blend Containing Triphenyl Phosphate and Nanoclay and Its Correlation with Morpholgy. *J. Appl. Polym. Sci.* **2010**, *118*, 1796–1804.
25. He, X.J.; Wang, L.J.; Xie, X.L.; Zhang, K. Investigation of thermal property and flame retardancy of ABS/montmorillonite nanocomposites. *Plast. Rubber Compos.* **2010**, *39*, 54–60. [CrossRef]
26. Ambre, A.; Jagtap, R.; Dewagan, B. ABS Nanocomposites Containing Modified Clay. *J. Reinf. Plast. Comp.* **2009**, *28*, 343–352. [CrossRef]
27. Lim, S.K.; Hong, E.P.; Song, Y.H.; Park, B.J.; Choi, H.J.; Chin, I.J. Preparation and Interaction Characteristics of Exfoliated ABS/Organoclay Nanocomposite. *Polym. Eng. Sci.* **2010**, *50*, 504–512. [CrossRef]
28. Sanchez, S.; Ibarra, R.; Solis, F.; Cordoba, L. Conventional Processing and Rheology of Nanocomposites ABS/Montmorillonite. *ANTEC* **2009**, *1*, 453–459.
29. Patino-Soto, A.P.; Sanchez-Valdes, S.; Ramos-DeValle, L.F. Morphological and Thermal Properties of ABS/Montmorillonite Nanocomposites Using Two Different ABS Polymers and Four Different Montmorillonite Clays. *J. Polym. Sci. Part B Polym. Phys.* **2008**, *46*, 190–200. [CrossRef]
30. Lee, K.M.; Han, C.D. Effect of hydrogen bonding on the rheology of polycarbonate/organoclay nanocomposites. *Polymer* **2003**, *44*, 4573–4588. [CrossRef]
31. Saadat, A.; Nazockdast, H.; Sepehr, F.; Mehranpour, M. Linear and Nonlinear Melt Rheology and Extrudate Swell of Acrylonitrile-Butadiene-Styrene and Organoclay-Filled Acrylonitrile-Butadiene-Styrene Nanocomposite. *Polym. Eng. Sci.* **2010**, *50*, 2340–2349. [CrossRef]
32. Ozkaraca, A.C.; Kaynak, C. Contribution of Nanoclays to the Performance of Traditional Flame Retardants in ABS. *Polym. Comp.* **2012**, *33*, 420–429. [CrossRef]
33. Wang, S.; Hu, Y.; Song, L.; Liu, J.; Chen, Z.; Fan, W. Study on the Dynamic Self-Organization of Montmorillonite in Two Phases. *J. Appl. Polym. Sci.* **2004**, *91*, 1457–1462. [CrossRef]
34. Bourbigot, S.; Vanderhart, D.L.; Gilman, J.W.; Bellayer, S.; Stretz, H.; Paul, D.R. Solid state NMR characterization and flammability of styrene-acrylonitrile copolymer montmorillonite nanocomposite. *Polymer* **2004**, *45*, 7627–7638. [CrossRef]
35. Zhang, J.; Jiang, D.D.; Wang, D.; Wilkie, C.A. Styrenic polymer nanocomposites based on an oligomerically-modified clay with high inorganic content. *Polym. Degrad. Stab.* **2006**, *91*, 2665–2674. [CrossRef]
36. Kim, H.-S.; Park, B.H.; Choi, J.H.; Yoon, J.-S. Preparation and Mechanical Properties of Acrylonitrile-Butadiene-Styrene Copolymer/Clay Nanocomposites. *J. Appl. Polym. Sci.* **2008**, *107*, 2539–2544. [CrossRef]
37. Guo, T.; Hao, G.; Song, M.; Zhang, B. Amphiphilic Poly(styrene-b-ethlene oxide)-Block-Compolymer-Intercalated Layered Silicate and Its Nanocomposites with Acrylonitrile-Butadiene-Styrene Resin. *J. Appl. Polym. Sci.* **2004**, *94*, 238–242. [CrossRef]
38. Nayak, S.K.; Mohanty, S.; Samal, S.K. Mechanical and Thermal Properties Enhancement of Polycarbonate Nanocomposites Prepared by Melt Compounding. *J. Appl. Polym. Sci.* **2010**, *117*, 2101–2112. [CrossRef]
39. Choi, Y.S.; Xub, M.; Chung, I.J. Synthesis of exfoliated acrylonitrile-butadiene-styrene copolymer (ABS) clay nanocomposites: Role of clay as a colloidal stabilizer. *Polymer* **2005**, *46*, 531–538. [CrossRef]
40. Liu, M.; Zhang, X.; Zammarano, M.; Gilman, J.W.; Davis, R.D.; Kashiwagi, T. Effect of montmorillonite dispersion on flammability properties of poly(styrene-co-acrylonitrile) nanocomposites. *Polymer* **2011**, *52*, 3092–3103. [CrossRef]
41. Mainil, M.; Urbanczyk, L.; Calberg, C.; Germain, A.; Jerome, C.; Bourbigot, S.; Devaux, J.; Sclavons, M. Morphology and Properties of SAN-Clay Nanocomposites Prepared Principally by Water-Assisted Extrusion. *Polym. Eng. Sci.* **2010**, *50*, 10–21. [CrossRef]
42. Tiwari, R.R.; Natarajan, U. Effect of Organic Modifiers and Silicate Type on Filler Dispersion, Thermal, and Mechanical Properties of ABS-Clay Nanocomposites. *J. Appl. Polym. Sci.* **2008**, *110*, 2374–2383. [CrossRef]
43. Modesti, M.; Besco, S.; Lorenzetti, A.; Zammarano, M.; Causin, V.; Marega, C.; Gilman, J.W.; Fox, D.M.; Trulove, P.C.; De Long, H.C.; et al. Imidazolium-modified clay-based ABS nanocomposites: A comparison between melt-blending and solution-sonication processes. *Polym. Adv. Technol.* **2008**, *19*, 1576–1583. [CrossRef]
44. Modesti, M.; Besco, S.; Lorenzetti, A.; Causin, V.; Marega, C.; Gilman, J.W.; Fox, D.M.; Trulove, P.C.; De Long, H.C.; Zammarano, M. ABS/clay nanocomposites obtained by a solution technique: Influence of clay organic modifiers. *Polym. Degrad. Stab.* **2007**, *92*, 2206–2213. [CrossRef]
45. Hameed, N.; Sreekumar, P.A.; Francis, B.; Yang, W.; Thomas, S. Morphology, dynamic mechanical and thermal studies on poly(styrene-co-acrylonitrile) modified epoxy resin/glass fibre composites. *Compos. Part A Appl. Sci. Manuf.* **2007**, *38*, 2422–2432. [CrossRef]
46. Callaghan, T.A.; Takakuwa, K.; Paul, D.R.; Padwa, A.R. Polycarbonate-SAN copolymer interaction. *Polymer* **1993**, *34*, 3796–3808. [CrossRef]
47. Skochdopole, R.E.; Finch, C.R.; Marshall, J. Properties and Morphology of Some Injection-Molded Polycarbonate-Styrene Acrylonitrile Copolymer Blends. *Polym. Eng. Sci.* **1987**, *27*, 627–631. [CrossRef]
48. Keitz, J.D.; Barlow, J.W.; Paul, D.R. Polycarbonate Blends with Styrene/Acrylonitrile Copolymers. *J. Appl. Polym. Sci.* **1984**, *29*, 3131–3145. [CrossRef]

49. Kim, W.N.; Burns, C.M. Thermal Behavior, Morphology, and Some Melt Properties of Blends of Polycarbonate with Poly(Styrene-Co-Acrylonitrile) and Poly(Acrylonitrile-Butadiene-Styrene). *Polym. Eng. Sci.* **1988**, *28*, 1115–1127. [CrossRef]
50. Huang, J.-C.; Wang, M.-S. Recent Advances in ABS/PC Blends. *Adv. Polym. Technol.* **1989**, *9*, 293–299. [CrossRef]
51. Kim, W.Y.; Lee, D.S. Morphology and mechanical property of the polycarbonate/poly(styrene-co-acrylonitrile) blend containing poly(e-caprolactone). *Polym. Bull.* **1991**, *26*, 701–707. [CrossRef]